A Theoretical and Experimental Study on the Lewis Acid−Base Adducts $(P_4E_3)\cdot(BX_3)$ (E = S, Se; X = Br, I) and $(P_4Se_3)\cdot(NbCl_5)$

Christoph Aubauer, Elisabeth Irran, Thomas M. Klapötke,* Wolfgang Schnick, Axel Schulz, and Jürgen Senker

Department of Chemistry, Ludwig-Maximilians-University, Butenandtstr. 5-13 (D), D-81377 Munich, Germany

Received December 7, 2000

The Lewis acid−base adducts $(P_4E_3)\cdot(BX_3)$ (E = S, Se; X = Br, I) and $(P_4Se_3)\cdot(NbCl_5)$ have been prepared and characterized by Raman, IR, and solid-state ^{31}P MAS NMR spectroscopy. Hybrid density functional calculations (B3LYP) have been carried out for both the apical and the basal $(P_4E_3)\cdot(BX_3)$ (E = S, Se; X = Br, I) adducts. The thermodynamics of all considered species has been discussed. In accordance with solid-state ^{31}P MAS NMR and vibrational data, the X-ray powder diffraction structures of $(P_4S_3)\cdot(BBr_3)$ [monoclinic, space group $P2_1/m$ (No. 11), $a = 8.8854(1)$ Å, $b = 10.6164(2)$ Å, $c = 6.3682(1)$ Å, $\beta = 108.912(1)°$, $V = 568.29(2)$ Å^3, $Z = 2$] and $(P_4S_3)\cdot(BI_3)$ [orthorhombic, space group *Pnma* (No. 62), $a = 12.5039(5)$ Å, $b = 11.3388(5)$ Å, $c = 8.9298(4)$ Å, $V = 1266.09(9)$ Å^3, $Z = 4$] indicate the formation of an apical P_4S_3 complex in the reaction of P_4S_3 with BX_3 (X = Br, I). Basal adducts are formed when P_4Se_3 is used as the donor species. Vibrational assignment for the normal modes of these adducts has been made on the basis of comparison between theoretically obtained and experimentally observed vibrational data.

Introduction

Previous work has shown that P_4S_3 and P_4Se_3 form weak 1:1 donor−acceptor complexes with Lewis acids.[1−4] These adducts show cage-like structures with three basal and one apical P atoms connected by three E (E = S, Se) atoms. From the electronic situation both the negatively charged apical and the three basal phosphorus atoms can act as donors.

X-ray structural investigations of the complexes $[Ni(P_4E_3)\cdot(tppea)]$ (tppea = tris(2-diphenylphosphinoethyl)amine)[1] and $[Mo(CO)_5]\cdot(P_4S_3)$[2] showed an intact P_4E_3 (E = S, Se) cage coordinated to the transition metal through the apical P atom. In case of $[IrCl(CO)(PPh_3)_2]$ the reaction with P_4S_3 leads to a cleavage of one P−P bond in the cage molecule yielding the dimeric complex $[Ir(\mu\text{-}P_4S_3)Cl(CO)(PPh_3)]_2$.[5] The reaction of $[Pt(C_2H_4)(PPh_3)_2]$ with P_4S_3 gives the trinuclear platinum complex $[\{Pt(\mu\text{-}P_4S_3)(PPh_3)\}_3]\cdot C_6H_6$ through insertion of the metal fragment into a P−P bond of the cage.[6] The crystal structures of $[Ir(\mu\text{-}P_4S_3)Cl(CO)(PPh_3)]_2$[5] and $[\{Pt(\mu\text{-}P_4S_3)(PPh_3)\}_3]\cdot C_6H_6$[6] showed that the metal atoms are linked to two "basal" phosphorus atoms of the P_4S_3 cage and one basal P atom of another P_4S_3 cage.

The reaction of $[MCl(cod)]_2$ (M = Rh, Ir; cod = cyclo-octa-1,5-diene) with P_4E_3 in the presence of tris(diphenylphosphinomethyl)ethane led to complexes of the type $[(triphos)M(P_3E_3)]$ (E = S, Se), in which the metal atom replaced one basal P atom of the original P_4E_3 cage.[7]

Goh and co-workers recently studied the reaction of $[CpCr(CO)_3]_2$ with P_4E_3 (E = S, Se) yielding $(Cp_4Cr_4(CO)_9)\cdot(P_4E_3)\cdot{}^1/_2C_6H_6$. The crystal structures of $(Cp_4Cr_4(CO)_9)\cdot(P_4E_3)\cdot{}^1/_2C_6H_6$ revealed an opened-up conformation of the P_4E_3 cage, containing one $CpCr(CO)_3$ and three $CpCr(CO)_2$ fragments coordinated to four P atoms of a five-membered ring.[8]

Blachnik et al. published the Lewis acid−base $(P_4Se_3)\cdot(NbCl_5)$ adduct obtained from the reaction of P_4Se_3 with $NbCl_5$. The crystal structure of $(P_4Se_3)\cdot(NbCl_5)$ showed that the Nb−P bond is formed between a basal phosphorus atom of the P_4Se_3 cage and the $NbCl_5$. In contrast to this species, $[\beta\text{-}(P_4S_4)\cdot(NbCl_5)_2]$ was obtained in the reaction of P_4S_3 with $NbCl_5$. In $[\beta\text{-}(P_4S_4)\cdot(NbCl_5)_2]$ two $NbCl_5$ units are coordinated to the basal phosphorus atoms.[3]

In summary, the versatile reactivity of the P_4E_3 cage molecules toward acceptor species can result in (i) a coordination of the intact cage to the ligand via its apical or basal P atoms,[2,3,4] (ii) an insertion of the ligand fragment into a P−P bond of the cage,[5,6,8] or (iii) substantial cleavage of the cage molecule yielding fragments such as P_2, P_3, P_2E, P_2E_2, P_3E_3, and E_4.[7,8]

We are interested in the bonding situation of P−B adducts,[4] and in this study we investigated the reactions of P_4E_3 (X = S, Se) with the boron trihalides BX_3 (X = Br, I). In particular, in

* To whom correspondence should be sent. E-mail: tmk@cup.uni-muenchen.de.

(1) (a) Di Vaira, M.; Peruzzini, M.; Stoppioni, P. *Inorg. Chem.* **1983**, *22*, 2196. (b) Di Vaira, M.; Peruzzini, M.; Stoppioni, P. *J. Organomet. Chem.* **1983**, *258*, 373.
(2) Cordes, A. W.; Joyner, R. D.; Shores, R. D.; Dill, E. D. *Inorg. Chem.* **1974**, *13*, 132.
(3) Nowottnick, H.; Stumpf, K.; Blachnik, R.; Reuter, H. *Z. Anorg. Allg. Chem.* **1999**, *625*, 693.
(4) Aubauer, Ch.; Klapötke, T. M.; Schulz, A. *J. Mol. Model.* **2000**, *6*, 76.
(5) Ghilardi, C. A.; Midollini, S.; Orlandini, A. *Angew. Chem., Int. Ed. Engl.* **1983**, *22*, 790.
(6) Di Vaira, M.; Peruzzini, M.; Stoppioni, P. *J. Chem. Soc, Dalton Trans.* **1983**, 291.
(7) Di Vaira, M.; Mann, B. E.; Peruzzini, M.; Stoppioni, P. *Inorg. Chem.* **1988**, *27*, 3725.
(8) (a) Goh, L. Y.; Chen, W.; Wong, R. C. S. *Organometallics* **1999**, *18*, 306. (b) Goh, L. Y.; Chen, W.; Wong, R. C. S. *Organometallics* **1995**, *14*, 3886. (c) Goh, L. Y.; Wei, C.; Wong, R. C. S. *Angew. Chem., Int. Ed. Engl.* **1993**, *32*, 1728. (d) Goh, L. Y.; Wei, C.; Wong, R. C. S. *Phosphorus Sulfur* **1994**, *93−94*, 209.

10.1021/ic001384x CCC: $20.00
Published on Web 08/17/2001

Table 1. Selected Calculated and Experimental Structural Data (distances in Å, angles in deg) for the Adducts $(P_4S_3)\cdot(BX_3)$ (X = Br, I)

	$(P_4S_3)\cdot(BBr_3)$ calculation		exp	$(P_4S_3)\cdot(BI_3)$ calculation		exp
	apical	basal	apical	apical	basal	apical
B−X(1)	1.997	2.004	2.16(3)	2.245	2.252	[2.250(1)][a]
B−X(2)	1.997	2.004	1.89(1)	2.245	2.252	[2.249(1)][a]
B−P(1)	2.085		2.01(3)	2.022		[2.020(1)][a]
B−P(2)		2.066			2.007	
P(1)−S(1)	2.129	2.150	2.042(8)	2.133	2.149	2.10(1)
P(1)−S(2)	2.129	2.162	2.006(6)	2.133	2.164	1.992(8)
P(2)−S(1)	2.132	2.112	2.06(1)	2.128	2.115	2.18(1)
P(3)−S(2)	2.132	2.132	2.162(6)	2.128	2.132	2.154(7)
P(2)−P(3)	2.291	2.243	2.247(8)	2.293	2.243	2.316(9)
P(3)−P(3A)	2.291	2.321	2.101(9)	2.293	2.328	2.37(1)
S(1)−P(1)−S(2)	102.8	100.0	103.3(3)	102.7	100.1	109.3(4)
P(2)−P(3)−P(3A)	60.0	58.8	62.1(2)	60.0	58.7	59.2(2)
P(3)−P(2)−P(3A)	60.0	62.3	55.7(3)	60.0	62.5	61.5(4)
X(1)−B−P(1)	104.1		98(1)	104.8		[106.4(4)][a]
X(1)−B−P(2)		101.4			101.6	
X(2)−B−P(1)	104.1		108.4(8)	104.8		[109.2(2)][a]
X(2)−B−P(2)		105.6			106.1	
X(1)−B−X(2)	114.3	114.0	108.6(8)	113.7	113.5	[110.5(1)][a]
X(2)−B−X(2A)	114.3	114.5	122(1)	113.7	114.3	[110.5(2)][a]

[a] P−B and B−I distances were fixed by soft constraint during the Rietveld refinement.

this contribution we want to address the question as to whether in the adducts $(P_4E_3)\cdot(BX_3)$ (E = S, Se; X = Br, I) the boron trihalide is linked via the apical or the basal phosphorus atom of the P_4E_3 cage. The Lewis acid−base complexes $(P_4E_3)\cdot(BX_3)$ (E = S, Se; X = Br, I) and the adduct $(P_4Se_3)\cdot(NbCl_5)$ were characterized by means of solid-state ^{31}P MAS NMR, IR, and Raman spectroscopy. Hybrid density functional calculations were carried out for both the apical and the basal Lewis acid−base adducts. The structures of $(P_4S_3)\cdot(BBr_3)$ and $(P_4S_3)\cdot(BI_3)$ have been established by ab initio X-ray powder diffraction. $(P_4Se_3)\cdot(NbCl_5)$ was used as a reference molecule in order to compare and confirm our experimental and theoretical findings on $(P_4E_3)\cdot(BX_3)$.

Results and Discussion

Pure yellow tetraphosphorus trisulfide boron triiodide, $(P_4S_3)\cdot(BI_3)$, was prepared from the reaction of one equivalent of P_4S_3 with one equivalent of BI_3, eq 1, in CS_2 at room temperature.

$$P_4S_3 + BI_3 \xrightarrow{CS_2} (P_4S_3)\cdot(BI_3) \qquad (1)$$

The BBr_3 adducts $(P_4S_3)\cdot(BBr_3)$ and $(P_4Se_3)\cdot(BBr_3)$ were obtained from the reaction of P_4E_3 (E = S, Se) with an excess of BBr_3 in CS_2, eq 2.

$$P_4E_3 + BBr_3 \xrightarrow{CS_2} (P_4E_3)\cdot(BBr_3)\ (E = S, Se) \qquad (2)$$

We tried to dissolve $(P_4S_3)\cdot(BI_3)$ in different solvents e.g. CS_2, CH_3CN, $CFCl_3$, and SO_2, however the solubility of $(P_4S_3)\cdot(BI_3)$ is very small. The saturated solution in CS_2 contains essentially only very small amounts of P_4Se_3 and BI_3 as indicated by ^{31}P and ^{11}B NMR studies.

In contrast, the complexes $(P_4S_3)\cdot(BBr_3)$ and $(P_4Se_3)\cdot(BBr_3)$ are very soluble in common solvents, however, the ^{31}P and ^{11}B NMR spectra showed resonances for P_4E_3 (E = S, Se) and BBr_3. Therefore, it can be assumed that these P−B complexes exist only in the solid-state.

Structure. The molecular structures of both the apical and the basal $(P_4E_3)\cdot(BX_3)$ (E = S, Se; X = Br, I) were fully optimized at B3LYP level. All considered P−B adducts were shown to possess stable minima at B3LYP level (no imaginary frequencies).

Structural parameters obtained from density functional theory (B3LYP) calculations for main group element compounds are in good agreement with those obtained from experimental studies. It is generally agreed that this level is sufficient to predict the relative stability of the isomers and will give reasonably reliable results for the equilibrium structures.[9] Both the electronic situation and thermodynamics should slightly favor the formation of basal $(P_4E_3)\cdot(BX_3)$ adducts (E = S, Se; X = Br, I) in the gas-phase (see Section Thermodynamics).[4]

Selected bond lengths and bond angles of $(P_4S_3)\cdot(BBr_3)$ and $(P_4S_3)\cdot(BI_3)$ obtained by ab initio X-ray powder diffraction in comparison with the computed structures are summarized in Table 1.

$(P_4S_3)\cdot(BBr_3)$ crystallizes in the monoclinic space group $P2_1/m$ with two molecules in the unit cell (Figure 1). The X-ray structure determination revealed an intact P_4S_3 cage linked via an apical P atom to the BBr_3 acceptor unit.

Two different B−Br [B−Br(1), B−Br(2)], P_{ap}−S [P(1)−S(1), P(1)−S(2)], S−P_{bas} [S(1)−P(2), S(2)−P(3)], and P−P [P(2)−P(3), P(3)−P(3A)] bond lengths (Figure 1) were found for the C_s symmetric $(P_4S_3)\cdot(BBr_3)$ molecule in the solid-state. The orientation of the S and basal P atoms of the P_4S_3 cage and the Br atoms of the BBr_3 moiety shows a slightly distorted staggered conformation. In contrast, the computed structure of $(P_4S_3)\cdot(BBr_3)$ predicts C_{3v} symmetry in the gas-phase with a staggered conformation. Hence, it is assumed that in solid-state the symmetry is lowered from C_{3v} to C_s due to crystal package effects and results in fairly large differences in the structural data between experiment and theory (Table 1).

Comparison of the structural data of coordinated P_4S_3 with the isolated P_4S_3 molecule shows that the bond angles of P_4S_3 have not considerably changed upon complexation. However, the values of the different P−P (2.247(8) and 2.101(9) Å), P_{bas}−S (2.06(1) and 2.162(6) Å), and P_{ap}−S (2.042(8) and 2.006(6) Å) bond lengths display large deviations from the bond lengths in the isolated P_4S_3 molecule resulting always in a longer and a shorter bond distance.

(9) Klapötke, T. M.; Schulz, A. *Quantum Chemical Methods in Main-Group Chemistry with an invited chapter by Harcourt, R. D.*; Wiley & Sons: Chichester, 1998.

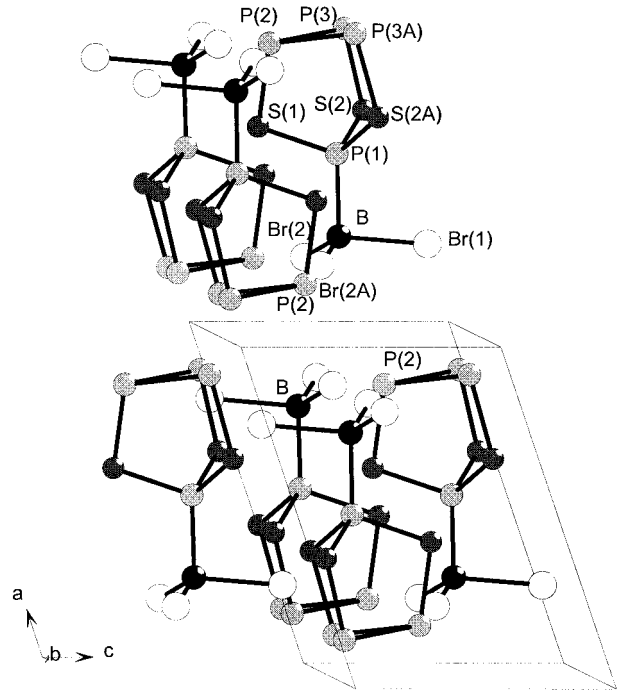

Figure 1. Unit cell of $(P_4S_3)\cdot(BBr_3)$ (X-ray powder diffraction).

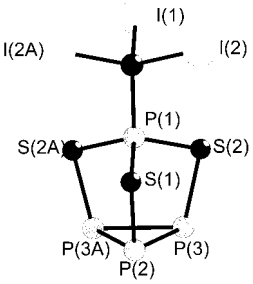

Figure 2. Molecular structure of $(P_4S_3)\cdot(BI_3)$ (X-ray powder diffraction).

The P−B bond length for $(P_4S_3)\cdot(BBr_3)$, which was found to be 2.01(3) Å, is in agreement with the P−B bond distance found in $Br_3P\cdot BBr_3$ (2.01(2) Å).[10]

Due to the observed C_s symmetry in $(P_4S_3)\cdot(BBr_3)$ two different B−Br bond lengths were found: two fairly short distances (1.89(1) Å) and one long distance (2.16(2) Å), which is significantly longer than in BBr_3 (gas electron diffraction: 1.893(5) Å[11]).

$(P_4S_3)\cdot(BI_3)$ crystallizes in the orthorhombic space group *Pnma* with four molecules in the unit cell (Figures 2 and 3).

Analogous to the $(P_4S_3)\cdot(BBr_3)$ molecular structure, the X-ray powder diffraction structural analysis of $(P_4S_3)\cdot(BI_3)$ shows the formation of an C_s symmetric apical adduct. Analogous to $(P_4S_3)\cdot(BBr_3)$, two different $S-P_{ap}$, $S-P_{bas}$, and P−P bond distances were found. As for $(P_4S_3)\cdot(BBr_3)$, B3LYP calculations also predict C_{3v} symmetry with equal P−P, P−S, and B−I bond distances.

Due to the three strong scattering iodine atoms, surrounding the boron atom, the position of the relatively light boron atom in $(P_4S_3)\cdot(BI_3)$ could not be exactly determined. Therefore, the P−B and B−I distances were fixed with soft constraints during the Rietveld refinement utilizing the computed B3LYP distances.

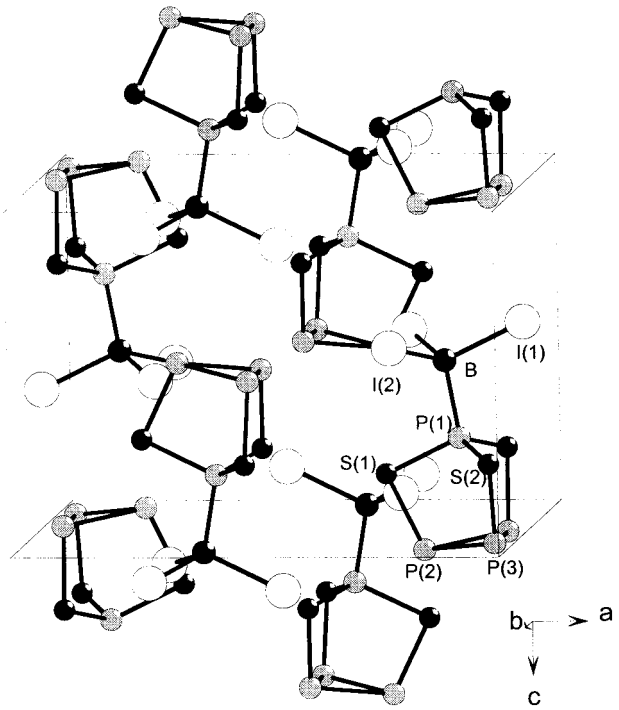

Figure 3. Unit cell of $(P_4S_3)\cdot(BI_3)$ (X-ray powder diffraction).

Table 2. Selected Calculated and Experimental Structural Data (distances in Å, angles in deg) for $(P_4Se_3)\cdot(NbCl_5)$

	calculation	X-ray[a]		calculation	X-ray[a]
P(1)−Se(1)	2.299	2.253(5)	Se(1)−P(1)−Se(3)	103.9	99.6(7)
P(1)−Se(3)	2.287	2.248(5)	Se(1)−P(1)−Se(2)	100.0	99.74(3)
P(2)−Se(3)	2.277	2.235(3)	Se(3)−P(4)−Nb	118.4	115.83(3)
P(4)−Se(3)	2.360	2.222(3)	P(1)−Se(1)−P(2)	100.2	100.8(6)
P(2)−P(3)	2.289	2.238(8)	P(1)−Se(3)−P(4)	97.3	97.3(1)
P(2)−P(4)	2.247	2.198(2)	P(2)−P(4)−Se(3)	108.9	109.6(0)
P(3)−P(4)	2.247	2.208(4)	P(4)−P(2)−Se(2)	103.5	102.75(5)
P(4)−Nb	2.909	2.778(2)	P(2)−P(4)−P(3)	61.2	61.1(2)
Nb−Cl(5)	2.289	2.270(6)	P(2)−P(3)−P(4)	59.3	59.26(0)
Nb−Cl(1)	2.367	2.314(9)	P(3)−P(2)−P(4)	59.3	59.7(2)
Nb−Cl(2)	2.359	2.301(3)	P(2)−P(4)−Nb	123.2	126.6(0)
			Cl(5)−Nb−P(4)	178.6	177.98(7)

[a] See ref 3.

The computed structural data (B3LYP) predict P−B distances of 2.085 Å $[(P_4S_3)\cdot(BBr_3)]$ and 2.022 Å $[(P_4S_3)\cdot(BI_3)]$, respectively, for the apical P_4S_3 adducts which are comparable with literature values for weak P−B Lewis acid−base complexes.[10,12]

In Table 2 selected computed and experimental structural data of the basal $(P_4Se_3)\cdot(NbCl_5)$ adduct (Figure 4) are summarized. All calculated structural parameters are in reasonable agreement with the data obtained by X-ray crystal structure determination. Bond lengths and angles in the P_4Se_3 fragment are comparable with the noncoordinated P_4Se_3 molecule.[13] The geometry around the Nb atom can be described as a slightly distorted octahedral arrangement. The four equatorial Cl atoms are bent toward the P_4Se_3 ligand. This structural feature can be partly attributed to the fairly long calculated P−Nb bond distance of 2.909 Å (B3LYP). As for $(P_4S_3)\cdot(BBr_3)$ a considerable deviation from the experiment was found for the P−Nb distance (X-ray: 2.778(2) Å).[3]

In Table 3 the calculated structural parameters for both the apical and the basal $(P_4Se_3)\cdot(BX_3)$ (X = Br, I) complexes are

(10) Aubauer, Ch.; Engelhardt, G.; Klapötke, T. M.; Nöth, H.; Schulz, A.; Warchhold, M. *Eur. J. Inorg. Chem.*, **2000**, 2245.
(11) Konaka, S.; Ito, T.; Morino, Y. *Bull. Chem. Soc. Jpn.* **1966**, *39*, 1146.
(12) Aubauer, Ch.; Davidge, K.; Klapötke, T. M.; Mayer, P.; Piotrowski, H.; Schulz, A. *Z. Anorg. Allg. Chem.*, **2000**, *626*, 2373.
(13) Vos, A.; Keulen, E. *Acta Crystallogr.* **1957**, *11*, 615.

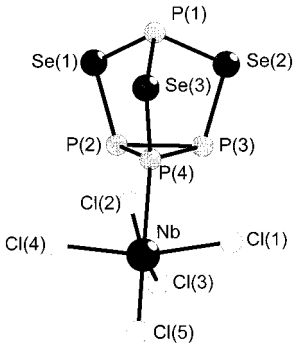

Figure 4. Calculated structure for $(P_4Se_3)\cdot(NbCl_5)$.

Table 3. Selected Calculated Structural Data (distances in Å, angles in deg) for the Adducts $(P_4Se_3)\cdot(BX_3)$ (X = Br, I)

	$(P_4Se_3)\cdot(BBr_3)$ calculation		$(P_4Se_3)\cdot(BI_3)^a$ calculation	
	apical	basal	apical	basal
B−X(1)	2.000	2.000	2.248	2.263
B−X(2)	2.000	2.248	2.248	2.243
B−P(1)	2.088		2.029	
B−P(4)		2.070		2.016
P(1)−Se(1)	2.302	2.322	2.308	2.327
P(1)−Se(3)	2.302	2.310	2.308	2.311
P(2)−Se(1)	2.299	2.300	2.296	2.300
P(4)−Se(3)	2.299	2.280	2.296	2.291
P(2)−P(3)	2.280	2.304	2.282	2.307
P(2)−P(4)	2.280	2.236	2.282	2.238
Se(1)−P(1)−Se(2)	103.0	99.3	102.9	99.9
P(2)−Se(1)−P(1)	96.0	100.2	95.9	100.3
P(4)−Se(3)−P(1)	96.0	95.5	95.9	95.4
P(2)−P(4)−P(3)	60.0	62.0	60.0	62.1
P(4)−P(2)−P(3)	60.0	59.0	60.0	59.0
X(1)−B−P(1)	104.4		105.1	
X(1)−B−P(4)		102.7		102.8
X(2)−B−P(1)	104.4		105.1	
X(2)−B−P(4)		105.3		106.1
X(1)−B−X(2)	114.0	113.9	113.5	113.2

[a] See ref 4.

listed. The apical adducts possess C_{3v} symmetry, in the basal adducts the symmetry is lowered to C_s symmetry. All structural parameters are in good agreement with those of other covalent Se−P compounds and P−B adducts.[3,10,12] As expected for these covalently bound P−B adducts both $(P_4Se_3)\cdot(BX_3)$ (X = Br, I) adducts display only a slight change in geometry compared with the starting material P_4Se_3.[4] The Se−P bond distances are slightly shorter in the adducts which stems from orbital contraction due to the increased positive charge in the P_4Se_3 unit.

The estimated B−P bond distances in both the apical [$(P_4Se_3)\cdot(BBr_3)$: 2.088 Å; $(P_4Se_3)\cdot(BI_3)$: 2.029 Å] and the basal [$(P_4Se_3)\cdot(BBr_3)$: 2.070 Å; $(P_4Se_3)\cdot(BI_3)$: 2.061 Å] adducts are comparable with the experimental value found in $(P_4S_3)\cdot(BBr_3)$ (1.99(3) Å), however, significantly longer than in $Me_3P\cdot BBr_3$ (1.924(12) Å) and $Me_3P\cdot BI_3$ (1.918(15) Å),[14] corresponding to a bond order less than 1. This can be explained by the larger electron transfer within $Me_3P\cdot BX_3$ (X = Br, I) due to the positive inductive effect of the methyl groups whereas in case of $(P_4Se_3)\cdot(BBr_3)$ and $(P_4Se_3)\cdot(BI_3)$ the donor strength is decreased.

Despite many attempts we were not able to solve the molecular structure of the adducts $(P_4Se_3)\cdot(BX_3)$ (X = Br, I) by means of X-ray powder diffraction, however, the solid-state ^{31}P MAS NMR and vibrational results (see below) indicate that both species represent basal complexes.

It is known that for adducts in solid-state and gas-phase structural data can be quite different. Leopold et al. have indicated that the dative or coordinate bond is much shorter in the solid-state than in the gas-phase, and this change has been associated with the substantial dipole moment of the adduct.[15] The calculated dipole moments of the P_4S_3 adducts show larger dipole moments for the apical species [e.g., $(P_4S_3)\cdot(BI_3)$: 5.74 D (apical) vs 3.58 D (basal)] which may indicate the preference of the apical adduct over the basal adduct formation in solid-state. In contrast to the P_4S_3 adducts, the magnitude of the dipole moments for P_4Se_3 adducts show an opposite trend [e.g., $(P_4Se_3)\cdot(BI_3)$: 2.58 D (apical) vs 5.33 D (basal)] which is in agreement with our experimental observation of the basal P_4Se_3 adducts.

Solid-State ^{31}P MAS NMR Results. Solid-state ^{31}P MAS NMR spectra were recorded of $(P_4E_3)\cdot(BX_3)$ (E = S, Se; X = Br, I), $(P_4Se_3)\cdot(NbCl_5)$ and P_4S_3 for reference using a single pulse acquisition and spinning speeds up to 35 kHz. The central peaks of the complex in each compounds were located by variation of the spinning frequency.

Table 4 summarizes the isotropic chemical shifts (δ) of all considered species and relative signal intensities obtained from spectra deconvolutions.

The solid-state ^{31}P MAS NMR spectrum of P_4S_3 shows one sharp resonance at $\delta = 78.4$ ppm due to the apical P and one broad resonance at $\delta = -105.1$ ppm due to the basal P atoms in a ratio of 1:3 (cf. δ (P_{ap}) = 71 ppm and δ (P_{bas}) = −120 ppm in solution[16]).

The ^{31}P MAS NMR spectra of $(P_4S_3)\cdot(BBr_3)$ and $(P_4S_3)\cdot(BI_3)$ are displayed in Figure 5. Besides impurities of P_4S_3 two central peaks in a ratio of 1:3 were observed in the ^{31}P MAS NMR spectrum of $(P_4S_3)\cdot(BBr_3)$ which can be assigned to the apical ($\delta = 135.2$ ppm) and the basal ($\delta = -109.8$ ppm) phosphorus atoms of $(P_4S_3)\cdot(BBr_3)$. Upon coordination, the ^{31}P resonance for the basal phosphorus atoms are slightly shifted to high field. The strong high frequency ^{31}P shift of roughly $\delta = +57$ ppm for the resonance of the apical phosphorus atom of $(P_4S_3)\cdot(BBr_3)$ compared with those of P_4S_3 indicates the formation of an apical adduct.

The ^{31}P NMR MAS spectrum of $(P_4S_3)\cdot(BI_3)$ (Figure 5) shows that the sample contained only small amounts of P_4S_3 impurities. The resonance at $\delta = 129.6$ ppm is due to the apical and the two resonances at $\Delta\delta = -92.0$ and −96.6 ppm are due to the basal phosphorus atoms. The relative intensity of the basal P atoms in a ratio of 2:1 is in agreement with the X-ray powder diffraction structure showing crystallographically unequal basal P nuclei. The coordination shift [$\Delta\delta_{coord} = \delta$ P(adduct) − δ P(P_4S_3)] of the apical phosphorus atom ($\Delta\delta_{coord} = +51.2$ ppm) in $(P_4S_3)\cdot(BI_3)$ is comparable with that found for $(P_4S_3)\cdot(BBr_3)$ ($\Delta\delta_{coord} = +56.8$).

The spectra of $(P_4S_3)\cdot(BX_3)$ (X = Br, I) show intense sidebands for the basal phosphorus atoms even at spinning

(14) Black, D. L.; Taylor, R. C. *Acta Crystallogr*. **1975**, *B31*, 1116.

(15) (a) Fiacco, D. L.; Mo, Y.; Hunt, S. W.; Ott, M. E.; Roberts, A.; Leopold, K. R. *J. Phys. Chem. A* **2001**, *105*, 484. (b) Fiacco, D. L.; Torro, A.; Leopold, K. R. *Inorg. Chem.* **2000**, *39*, 37. (c) Fiacco, D. L.; Hunt, S. W. Leopold, K. R. *J. Phys. Chem. A* **2000**, *104*, 8323. (d) Burns, W. A.; Phillips, J. A.; Canagaratna, M.; Goodfriend, H.; Leopold, K. R. *J. Phys. Chem. A* **1999**, *103*, 7445. (e) Canagaratna, M.; Phillips, J. A.; Goodfriend, H.; Leopold, K. R. *J. Am. Chem. Soc.* **1996**, *118*, 5290. (f) Leopold, K. R.; Canagaratna, M.; Phillips, J. A. In *Advances in Molecular Structure Research*; Hargittai, M.; Hargittai, I., Eds.; JAI Press: Greenwich, CT, 1996; Vol 2. p 103.

(16) (a) Dwek, R. A.; Richards, R. E.; Taylor, D.; Penney, G. J.; Sheldrick, G. M. *J. Chem. Soc. A* **1969**, 935. (b) Kolditz, L.; Wahner, E. *Z. Chem.* **1972**, *12*, 389.

Table 4. ^{31}P NMR Isotropic Shifts and Relative Intensities for P_4E_3, $(P_4E_3)\cdot(BX_3)$ (E = S, Se; X = Br, I), and $(P_4Se_3)\cdot(NbCl_5)$

	δ P_{ap} [ppm] coordinated	rel int	$\Delta\delta_{coord}$[a]	δ P_{ap} [ppm] noncoordinated	rel int	$\Delta\delta_{coord}$[a]	δ P_{bas} [ppm] coordinated	rel int	$\Delta\delta_{coord}$[a]	δ P_{bas} [ppm] noncoordinated	rel int	$\Delta\delta_{coord}$[a]
P_4S_3				78.4	1					−105.1	3	
$(P_4S_3)\cdot(BBr_3)$	135.2	1	+56.8							−109.8	3	−4.7
$(P_4S_3)\cdot(BI_3)$	129.6	1	+51.2							−92.0/−96.6	2:1	+ 13.1/+ 8.5
P_4Se_3[b]				90.1/86.5/68.1	1:2:1					−64.4	12	
$(P_4Se_3)\cdot(NbCl_5)$				72.2	1	−14.3[c]	−0.2	1	+64.2	−97.9/−99.8	1:1	−33.5/−35.4
$(P_4Se_3)\cdot(BBr_3)$				121.9/103.9	2:1	+35.4/+17.4[c]	39.7	2	+104.1	−82.5/−94.3	7	−18.1/−29.9
$(P_4Se_3)\cdot(BI_3)$				126.6	1	+40.1[c]	112.6	1	+177.0	−84.2	2	−19.8

[a] $\Delta\delta_{coord} = \delta$ P(adduct) − δ P(P_4E_3). [b] See ref 17. [c] $\Delta\delta_{coord}$ referring to δ (P_{ap} (P_4Se_3)) = 86.5 ppm.

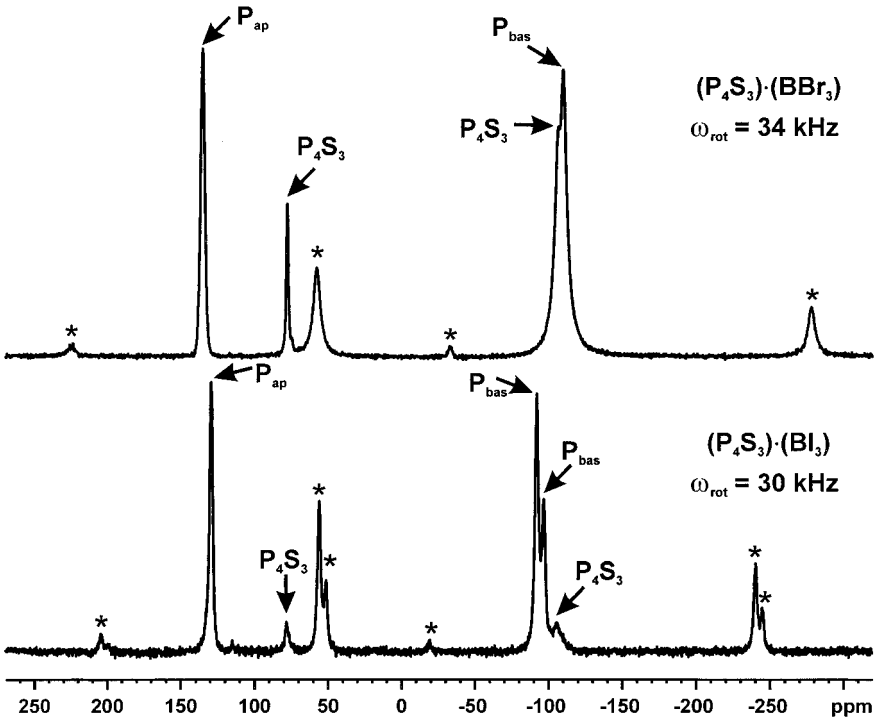

Figure 5. ^{31}P MAS NMR spectra of $(P_4S_3)\cdot(BBr_3)$ and $(P_4S_3)\cdot(BI_3)$. The central lines are indicated by arrows, asteriks denote spinning sidebands.

speeds more than 30 kHz. In contrast, only weak sidebands for the apical P atom were observed. This indicates that the chemical shift anisotropy associated with these atoms is considerably smaller than for the basal atoms. Also, since the apical atoms sit on the molecular C_s symmetry axis, its tensor should be axially symmetric.

The crystal structure of α-P_4Se_3 reported by Vos and Keulen contains four independent molecules with slightly different local environments for the individual P atoms.[13] Therefore, Lathrop and Eckert found three sharp patterns, centered at δ = 90.1, 86.5, and 68.1 ppm for the resonances of the apical P atoms in the ^{31}P MAS NMR spectrum of α-P_4Se_3.[17] The resonances for the basal P atoms are centered at δ = −64.4 ppm.

$(P_4Se_3)\cdot(NbCl_5)$ was shown to be a basal adduct.[3] The ^{31}P NMR MAS spectrum of $(P_4Se_3)\cdot(NbCl_5)$ (Figure 6) displays four signals in a ratio of 1:1:1:1. The sharp resonance at δ = 72.2 ppm and the two resonances at δ = −97.9 and −99.8 ppm can be assigned to the apical and the two noncoordinated basal phosphorus atoms. The broad pattern at δ = −0.2 ppm represents the resonance for the basal phosphorus atom coordinated to the $NbCl_5$ unit resulting in a coordination shift of +64.2 ppm. Additionally, the resonances for the noncoordinated basal P atoms are significantly shifted to upfield.

The interpretation of the recorded ^{31}P NMR MAS spectrum of $(P_4Se_3)\cdot(BBr_3)$ (Figure 6) is not as straightforward as the interpretation of the spectra of P_4S_3 adducts. The ^{31}P NMR spectrum indicates a more complex solid-state structure consisting of three P_4Se_3 units in which only two cages are coordinated to the BBr_3 ligand through the basal P atoms. Because of little impurities of P_4Se_3 in the sample as well as of the differences in line width and the occurrence of spinning sidebands, it is not easy to estimate relative intensities. The spectrum shows three central peaks at δ = 121.9, 103.9, and 39.7 ppm in an approximate ratio of 2:1:2 and two resonances at δ = −82.5 and −94.3 ppm, respectively. The resonance at δ = 121.9 ppm can be assigned to the apical P atom of the coordinated P_4Se_3 molecules, whereas the apical P atom of the noncoordinated P_4Se_3 molecule can be observed at δ = 103.9 ppm. The peaks at δ = −82.5 and −94.3 are attributed to the noncoordinated basal P atoms. The resonance at δ = 39.7 ppm, assigned to the coordinated basal P atom, shows a significant high-frequency shift ($\Delta\delta_{coord}$ = +104.1 ppm) compared to isolated P_4Se_3. This high-frequency shift is considerably larger than it is in $(P_4Se_3)\cdot(NbCl_5)$. This effect can be explained by the shorter P−B bond length (cf. d (P−B, $(P_4Se_3)\cdot(BBr_3)$) = 2.070 Å; d (P−Nb, $(P_4Se_3)\cdot(NbCl_5)$) = 2.909 Å; Tables 2 and 3)

The ^{31}P NMR MAS spectrum of $(P_4Se_3)\cdot(BI_3)$ (Figure 6) displays three broad peaks at δ = 126.6, 112.6, and −84.2 ppm in a ratio of 1:1:2 and clearly indicates the formation of an basal adduct. No impurities of P_4Se_3 were observed in the spectrum. The noncoordinated basal P atoms (δ = −84.2) are slightly

(17) Lathrop, D.; Eckert, H. *J. Phys. Chem.* **1989**, *93*, 7895.

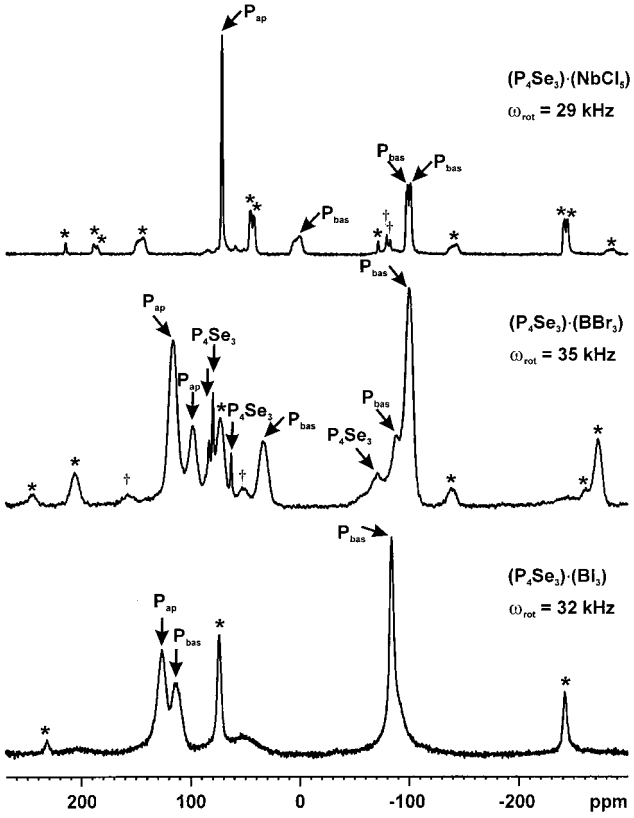

Figure 6. ^{31}P MAS NMR spectra of $(P_4Se_3)\cdot(BBr_3)$, $(P_4Se_3)\cdot(BI_3)$, and $(P_4Se_3)\cdot(NbCl_5)$. The central lines are indicated by arrows, asteriks denote spinning sidebands. Lines indicated by † originate from impurities.

shifted to low frequency. The peak at $\delta = 126.6$ ppm is very similar to the resonance of $(P_4Se_3)\cdot(BBr_3)$ (δ (P_{ap}) = 121.9 ppm) and can be attributed to the resonance of the apical phosphorus atom. The resonance at $\delta = 112.6$ ppm can be assigned to the basal phosphorus atom coordinated to the BI_3 ligand. On complexing, the downfield shift is largest for $(P_4Se_3)\cdot(BI_3)$ ($\Delta\delta_{coord} = +177.0$ ppm) corresponding to a stronger donor−acceptor interaction than in $(P_4Se_3)\cdot(BBr_3)$ and $(P_4Se_3)\cdot(NbCl_5)$.

To summarize, the reaction of P_4S_3 with BX_3 (X = Br, I) leads to apical adducts, whereas P_4Se_3 gives basal adducts. Upon coordination, the resonances are shifted to downfield. For apical adducts the coordination shift is in the range of +50 to +60 ppm, whereas no significant shift were observed for the basal atoms. For the basal adducts the downfield shift is significantly higher and decreases in the order $BI_3 > BBr_3 > NbCl_5$. Additionally, a small upfield shift of the ^{31}P resonances for noncoordinated basal phosphorus atoms could be observed. Moreover, the resonances of noncoordinated apical P atoms in $(P_4Se_3)\cdot(BX_3)$ (X = Br, I) are shifted to high frequency upon complexation.

Vibrational Spectroscopy. Figure 7 displays the Raman spectra of $(P_4S_3)\cdot(BBr_3)$ and $(P_4S_3)\cdot(BI_3)$ and Figure 8 the Raman spectra of $(P_4Se_3)\cdot(BBr_3)$, $(P_4Se_3)\cdot(BI_3)$, and $(P_4Se_3)\cdot(NbCl_5)$ (computed and experimentally observed vibrational frequencies and their approximate assignments of $(P_4E_3)\cdot(BX_3)$ (E = S, Se; X = Br, I) and $(P_4Se_3)\cdot(NbCl_5)$ are available as Supporting Information).

The theoretically predicted vibrational frequencies for $(P_4Se_3)\cdot(NbCl_5)$ and both possible Lewis acid−base adducts $(P_4E_3)\cdot(BX_3)$ (E = S, Se; X = Br, I) have been calculated with the harmonic approximation. The experimental vibrational data show the best agreement for apical adducts for $(P_4S_3)\cdot(BX_3)$ (X = Br, I) and basal adducts for $(P_4Se_3)\cdot(BX_3)$ (X = Br, I) and allow assignment. The deviation from experimentally obtained frequencies may partly be compensated by using scaling factors. It should be noted that the computation was carried out for a single, isolated (gas-phase) molecule. There may well be significant differences between gas-phase and solid-state spectra.

The broad peaks in the Raman spectra of $(P_4S_3)\cdot(BBr_3)$ and $(P_4Se_3)\cdot(BBr_3)$ in the range of ca. 600−660 cm^{-1} represent the asymmetric stretching vibration of the BBr_3 unit in the complex. The asymmetric B−I stretching mode can be observed in the Raman spectra of $(P_4S_3)\cdot(BI_3)$ and $(P_4Se_3)\cdot(BI_3)$ in the range of ca. 500−580 cm^{-1} (broad and weak peaks). In contrast to the Raman spectra, very intense peaks can be assigned to this ν_{as} (BX_3) vibration in the IR spectra.

The almost purely P−B stretching vibration can be observed at about 531 [$(P_4S_3)\cdot(BBr_3)$], 522 [$(P_4Se_3)\cdot(BBr_3)$], 566 [$(P_4S_3)\cdot(BI_3)$], and 560 cm^{-1} [$(P_4Se_3)\cdot(BI_3)$].

The intense IR frequencies, assigned to a combination mode of symmetric stretching modes of the P_4E_3 cage and the boron halide units and an P−B stretching vibration ($P_b + P_a$ out-of-phase) can be observed at ca. 390 [$(P_4S_3)\cdot(BX_3)$ (X = Br, I)] and ca. 350 cm^{-1} [$(P_4Se_3)\cdot(BX_3)$ (X = Br, I)]. Similar combination modes ($P_b + P_a$ in-phase) can be observed at ca.

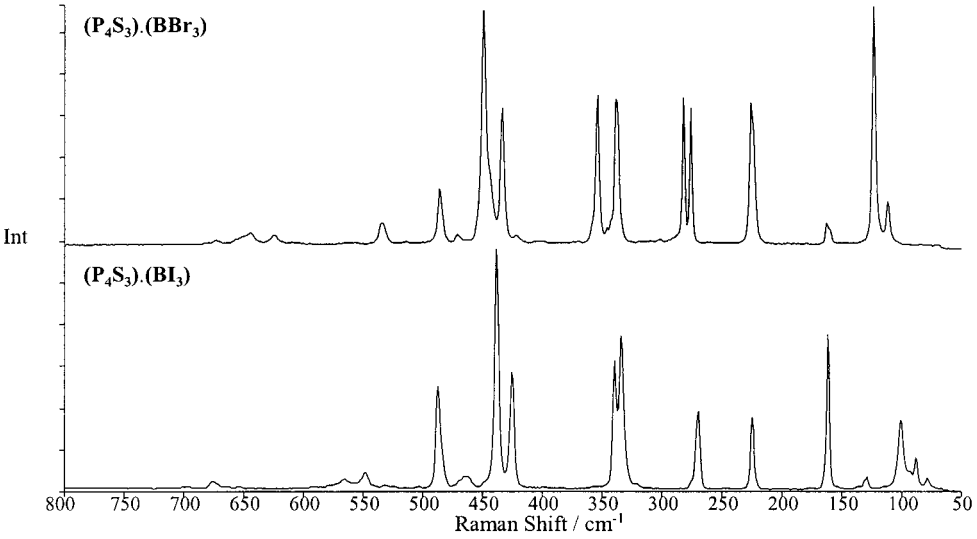

Figure 7. Raman spectra of $(P_4S_3)\cdot(BBr_3)$ and $(P_4S_3)\cdot(BI_3)$.

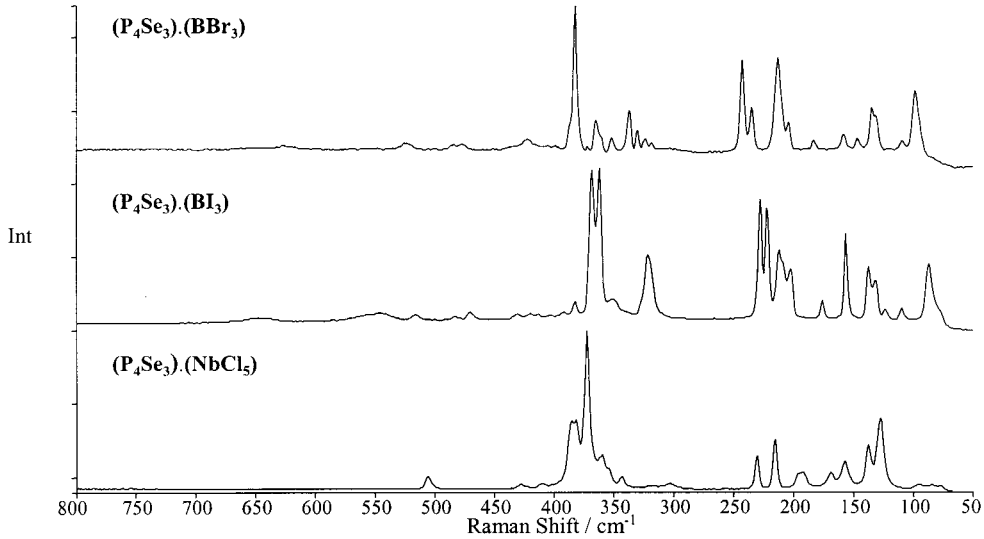

Figure 8. Raman spectra of $(P_4Se_3)\cdot(BBr_3)$, $(P_4Se_3)\cdot(BI_3)$, and $(P_4Se_3)\cdot(NbCl_5)$.

Table 5. Calculated Total Energies (E_{tot}) and Zero Point Vibrational Energies (*ZPE*) for P_4S_3, P_4Se_3, BBr_3, BI_3, $NbCl_5$, and Nb_2Cl_{10}

	P_4S_3	P_4Se_3[a]	BBr_3	BI_3[a]
point group	C_{3v}	C_{3v}	D_{3h}	D_{3h}
E_{tot} [a.u.]	−2560.089227	−1393.581226	−65.099012	−59.137598
NIMAG	0	0	0	0
ZPE [kcal mol^{-1}]	7.61	6.13	3.67	2.97

	$NbCl_5$	Nb_2Cl_{10}
point group	D_{3h}	D_{2h}
E_{tot} [a.u.]	−2358.216647	−4716.434741
NIMAG	0	0
ZPE [kcal mol^{-1}]	4.12	8.82

[a] See ref 4.

358 $[(P_4S_3)\cdot(BBr_3)]$, 338 $[(P_4S_3)\cdot(BI_3)]$, 322 $[(P_4Se_3)\cdot(BBr_3)]$, and 324 cm^{-1} $[(P_4Se_3)\cdot(BI_3)]$.

When comparing the experimentally observed wavenumbers with the theoretically predicted, a striking feature is the splitting of wavenumbers in the observed vibrational spectra of $(P_4Se_3)\cdot(BX_3)$ (X = Br, I) due to symmetry lowering from C_{3v} in isolated P_4Se_3 to C_s in basal P_4Se_3 adducts. This effect is less pronounced in the apical adducts.

Thermodynamics. Tables 5 and 6 summarize the total energies, electronic states and zero point vibrational energies of all considered species. At the considered level of theory (B3LYP) the adduct formation of $(P_4E_3)\cdot(BX_3)$ (E = S, Se; X = Br, I) represents an endothermic reaction in the gas-phase. In solid-state, the intermolecular interactions play an important role to stabilize these adducts and therefore needs to be considered. Chemically similar compounds are stabilized in the solid-state and this stabilization energy lies in the range of 25 ± 5 kcal mol^{-1}.[18] In addition, the reaction entropy has a large influence on the reaction (Table 6).

There is only a small difference in the Gibbs free energy of about 0.9 $[(P_4S_3)\cdot(BBr_3)]$, 1.7 $[(P_4S_3)\cdot(BI_3)]$, 1.9 $[(P_4Se_3)\cdot(BBr_3)]$, and 2.5 kcal mol^{-1} $[(P_4Se_3)\cdot(BI_3)]$ in favor of the basal adduct formation. The adduct formation of $(P_4E_3)\cdot(BX_3)(s)$ (E = S, Se; E = Br, I) is assumed to be a slightly exothermic reaction although these adducts are not thermodynamically stable in the gas-phase. Thermodynamics should favor the formation of basal P−B adducts. In contrast to these theoretical gas-phase results, the experimental data indicate that only the P_4Se_3 complexes represent basal adducts, whereas P_4S_3 forms apical adducts with BX_3 (X = Br, I) in the solid-state. Hence, small intermolecular interactions such as dipole−dipole interactions can determine which adduct is formed and explain the structural diversity of these adducts in the solid-state.

The formation of the $NbCl_5$ adduct, $(P_4Se_3)\cdot(NbCl_5)$, is estimated to be an exothermic process with −14.5 kcal mol^{-1} and Gibbs free energy of −4.6 kcal mol^{-1}. Since the adduct formation can be superimposed by an equilibrium reaction $NbCl_5/Nb_2Cl_{10}$, we have investigated the dimerization of $NbCl_5$ which however represents a slightly endothermic reaction (Tab. 9). Hence, the influence of the dimerization on the adduct formation is negligible.

Conclusions

As indicated by hybrid density functional calculations, the adduct formation of P_4E_3 (E = S, Se) with Lewis bases such as BX_3 (X = Br, I) and $NbCl_5$ is a process which is a borderline case between an endothermic and exothermic reaction. The two possible isomers, the apical and basal complexes a separated by a small energy gap of about 1−3 kcal mol^{-1} (in the gas phase).

Moreover, these phosphorus boron Lewis acid−base adducts represent "partially bound" systems, in which the P_4E_3 and BX_3 moieties are chosen to produce a dative linkage that is intermediate between a van der Waals interaction and a fully formed chemical bond.[15] These weakly bound complexes are extraordinarily sensitive to the presence of neighboring molecules resulting in significant changes in structure from gas-phase into solid-state. Hence, small intermolecular interactions such as van der Waals interactions can favor one (apical or basal) form and are responsible for the structural diversity in these adducts, e.g., symmetry decrease from the ideal C_{3v} to C_s for the P_4S_3 adducts and huge differences in bond distances.

According to the experimental results (solid-state ^{31}P MAS NMR, Raman, IR, X-ray powder diffraction), $(P_4S_3)\cdot(BBr_3)$ and $(P_4S_3)\cdot(BI_3)$ represent apical complexes, whereas P_4Se_3 forms basal adducts with BX_3 (X = Br, I) and $NbCl_5$ in the solid-state. Upon coordination, the ^{31}P MAS NMR resonances are shifted to downfield. For the apical P_4S_3 adducts the coordination

(18) Rossini, F. D.; Wagman, D. D.; Evans, W. H.; Levine, S.; Jaffe, I. *Selected Values of Chemical Thermodynamic Properties*; United States Government Printing Office: Washington, DC, 1952.

Table 6. Calculated Total Energies (E_{tot}), Zero Point Vibrational Energies (*ZPE*), Molar Enthalpy (ΔH_{298}), and Gibbs Free Energy (ΔG_{298}) for the Adduct Formation of $(P_4S_3)\cdot(BBr_3)$, $(P_4S_3)\cdot(BI_3)$, $(P_4Se_3)\cdot(BBr_3)$, $(P_4Se_3)\cdot(BI_3)$, and $(P_4Se_3)\cdot(NbCl_5)$

	$(P_4S_3)\cdot(BBr_3)$ apical	basal	$(P_4S_3)\cdot(BI_3)$ apical	basal
point group	C_{3v}	C_s	C_{3v}	C_s
E_{tot} [a.u.]	−2625.1602135	−2625.1615245	−2619.2022630	−2619.2049171
NIMAG	0	0	0	0
ZPE [kcal mol^{-1}]	11.80	11.73	11.25	11.18
ΔH_{298} [kcal·mol^{-1}]	18.67	17.81	16.65	14.94
ΔG_{298} [kcal·mol^{-1}]	29.22	28.12	27.59	25.61

	$(P_4Se_3)\cdot(BBr_3)$ apical	basal	$(P_4Se_3)\cdot(BI_3)$[a] apical	basal	$(P_4Se_3)\cdot(NbCl_5)$ basal
point group	C_{3v}	C_s	C_{3v}	C_s	C_s
E_{tot} [a.u.]	−1458.6698107	−1458.6729361	−1452.7120199	−1452.7161085	−3751.8229158
NIMAG	0	0	0	0	0
ZPE [kcal mol^{-1}]	10.13	10.18	9.56	9.61	10.82
ΔH_{298} [kcal·mol^{-1}]	7.55	5.61	5.43	2.89	−14.47[b]
ΔG_{298} [kcal·mol^{-1}]	17.82	15.91	15.66	13.06	−4.64[b]

[a] See ref 4. [b] $2\ NbCl_5 \rightarrow Nb_2Cl_{10}$ $\Delta H(298\ K) = 0.21$, $\Delta G(298\ K) = 12.07$ kcal·mol^{-1}.

shift is in the range of +50 to +60 ppm. For the basal P_4Se_3 adducts the downfield shift is significantly higher and decreases in the order $BI_3 > BBr_3 > NbCl_5$. The 2:1 splitting of the resonances for the basal phophorus atoms in the solid-state ^{31}P MAS NMR of $(P_4S_3)\cdot(BI_3)$ clearly indicates the occurrence of symmetry decrease from C_{3v} to C_s in solid-state.

Symmetry decrease from C_{3v} to C_s was also observed in the vibrational spectra of $(P_4Se_3)\cdot(BX_3)$. This effect less pronounced in the apical P_4S_3 adducts.

Experimental Section

Material and Apparatus. All of the compounds reported here are moisture sensitive. Consequently, strictly anaerobic and anhydrous conditions were employed for their syntheses. Any subsequent manipulations were carried out in a glovebox under dry nitrogen. BBr_3, BI_3, $NbCl_5$ (all Aldrich), and P_4S_3 (Fluka) were used as received. P_4Se_3 was prepared according to the literature.[3] The preparation of $(P_4Se_3)\cdot(BI_3)$[4] and $(P_4Se_3)\cdot(NbCl_5)$[3] also followed literature procedures. CS_2 was refluxed over P_4O_{10} and distilled prior to use.

^{31}P NMR spectra were measured at 202.49 MHz with a BRUKER DSX AVANCE 500 FT NMR spectrometer under fast spinning conditions about the magic-angle (MAS). A standard double-bearing MAS probe designed for zirconia dioxide 2.5 mm rotors was used with spinning frequencies up to 35 kHz. A single pulse acquisition with cycle observation was used and the 90°-pulse length was adjusted to 2 μs. The recycle delay was set to values between 5 and 1000 s depending of the spin lattice relaxation time to ensure correct relative signal intensities. Due to fast spinning conditions ($\nu_{rot} = 20-35$ kHz), the recorded spectra contain only few spinning sidebands which are clearly separated from the isotropic chemical shift resonances. Therefore, the values for the isotropic chemical shifts of the compounds under study could be extracted directly from the spectra without simulations taking into account the chemical shift anisotropy. Overlapping signals were deconvoluted using a Pseudo-Voigt profile. The samples were loaded under nitrogen atmosphere in a glovebox. The spectra were referenced to 85% H_3PO_4 in $CDCl_3$.

Raman spectra were obtained on powdered solid samples contained in glass capillary tubes with a Perkin-Elmer 2000 NIR spectrometer in the range 800−50 cm^{-1}. IR spectra were taken on Nujol mulls between CsI plates in the range 800−200 cm^{-1} on a Nicolet 520 FT IR spectrometer. For the determination of decomposition points, samples were heated in sealed glass capillaries in a Büchi B450 instrument.

Preparation of $(P_4S_3)\cdot(BI_3)$. $(P_4S_3)\cdot(BI_3)$ was prepared by addition of P_4S_3 (0.44 g, 2.00 mmol) in CS_2 to a solution of BI_3 (0.78 g, 2.00 mmol) in CS_2 at room temperature. A yellow precipitate formed immediately. After stirring for 15 min, the precipitate was separated by filtration and washed with CS_2 until the filtrate was colorless. Traces of CS_2 were removed under dynamic vacuum at room temperature. Yield: 0.99 g (81%) of yellow solid, mp 102 °C (decomp.).

Table 7. Crystallographic Data for $(P_4S_3)\cdot(BBr_3)$ and $(P_4S_3)\cdot(BI_3)$

	$(P_4S_3)\cdot(BBr_3)$	$(P_4S_3)\cdot(BI_3)$
formula	$BBr_3P_4S_3$	$BI_3P_4S_3$
M_w [g mol^{-1}]	470.64	611.62
crystal system	monoclinic	orthorhombic
space group	$P2_1/m$ (No. 11)	*Pnma* (No. 62)
diffractometer	STOE Stadi P (Cu Kα_1)	STOE Stadi P (Mo Kα_1)
λ [pm]	154.05	70.93
T [°C]	RT	RT
a [Å]	8.8854(1)	12.5039(5)
b [Å]	10.6164(2)	11.3388(5)
c [Å]	6.3682(1)	8.9298(4)
α [deg]	90	90
β [deg]	108.912(1)	90
γ [deg]	90	90
cell volume [Å^3]	568.29(2)	1266.06(9)
Z	2	4
profile range	$6° \le 2\theta \le 85°$	$3° \le 2\theta \le 54°$
no. data points	7800	4200
observed reflections	432	884
positional parameters	19	19
profile parameters	17	15
R_p	0.065	0.044
wR_p	0.083	0.056
R_F	0.072	0.064

Preparation of $(P_4S_3)\cdot(BBr_3)$. $(P_4S_3)\cdot(BBr_3)$ was prepared by addition of P_4S_3 (0.44 g, 2.00 mmol) in CS_2 to a solution of BBr_3 (0.53 g, 2.10 mmol) in CS_2 at room temperature. After cooling the reaction mixture to −78 °C, a yellow precipitate was formed. The precipitate was separated by filtration. Traces of CS_2 were removed under dynamic vacuum at room temperature. Yield: 0.83 g (88%) of yellow solid, mp 85 °C (decomp.).

Preparation of $(P_4Se_3)\cdot(BBr_3)$. $(P_4Se_3)\cdot(BBr_3)$ was prepared by addition of P_4Se_3 (0.57 g, 1.60 mmol) in CS_2 to a solution of BBr_3 (0.75 g, 3.00 mmol) in CS_2 at room temperature. After cooling the reaction mixture to −78 °C, a yellow precipitate was formed. The precipitate was separated by filtration. Traces of CS_2 were removed under dynamic vacuum at room temperature. Yield: 0.83 g (98%, calculated for $(P_4Se_3)_3\cdot(BBr_3)_2$) of yellow solid, mp 85 °C (decomp.).

X-ray Structure Determination. The X-ray diffraction measurements of $(P_4S_3)\cdot(BBr_3)$ and $(P_4S_3)\cdot(BI_3)$ were carried out in Debye−Scherrer geometry with glass capillaries on a STOE Stadi P powder diffractometer with Ge(111)-monochromatized radiation (Cu Kα_1 for $(P_4S_3)\cdot(BBr_3)$; Mo Kα_1 for $(P_4S_3)\cdot(BI_3)$). Indexing of the diffraction pattern was achieved with the program ITO.[19] From the systematic absences the space groups $P2_1$ or $P2_1/m$ for $(P_4S_3)\cdot(BBr_3)$ and $Pn2_1a$

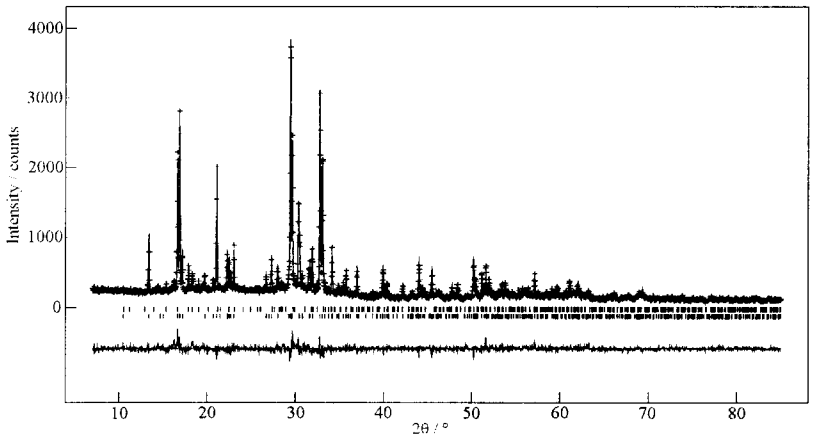

Figure 9. Observed (crosses) and calculated (line) X-ray powder diffraction pattern as well as difference profile of the Rietveld refinement of $(P_4S_3)\cdot(BBr_3)$. The lower row of vertical lines indicates possible peak positions of $(P_4S_3)\cdot(BBr_3)$, the upper row of P_4S_3. The powder pattern was obtained with a STOE Stadi P powder diffractometer (Cu Kα_1, λ = 154.05 pm).

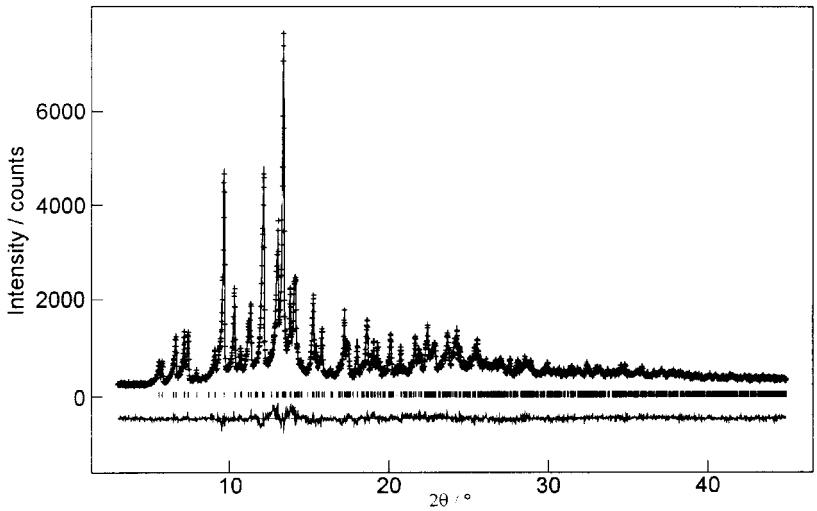

Figure 10. Observed (crosses) and calculated (line) X-ray powder diffraction pattern as well as difference profile of the Rietveld refinement of $(P_4S_3)\cdot(BI_3)$. The row of vertical lines indicates possible peak positions of $(P_4S_3)\cdot(BI_3)$. The powder pattern was obtained with a STOE Stadi P powder diffractometer (Mo Kα_1, λ = 70.93 pm).

or *Pnma* for $(P_4S_3)\cdot(BI_3)$ were considered. By assuming the respective centrosymmetric space group the position of all atoms of both compounds were determined ab initio by direct methods (programs EXTRA[20] and SIRPOW[21]). The Rietveld refinements of the crystal structures were performed with the program GSAS.[22] Small amounts of α-P_4S_3 were detected in the diffraction pattern of $(P_4S_3)\cdot(BBr_3)$. As in $(P_4S_3)\cdot(BI_3)$ the relatively light boron atom is surrounded by three atoms of the strongly scattering iodine, its position could not be determined with sufficient accuracy. Hence, the distances B−P and B−I had to be fixed with soft constraints during the refinement. The theoretical distances were taken from the hybrid density functional calculation. Detailed crystallographic data are summarized in Table 7, the refined parameters are listed in Tables 4 and 5 of the supporting material. The diffraction patterns of $(P_4S_3)\cdot(BBr_3)$ and $(P_4S_3)\cdot(BI_3)$ are illustrated in Figures 9 and 10.

Computational Methods. The structural and vibrational data of the considered species were calculated by using the hybrid density functional theory (B3LYP) with the program package Gaussian 98.[23] For phosphorus, sulfur and boron a standard 6-31G(d) basis set was used and for Br, I, and Se quasi-relativistic pseudopotentials (Br, ECP28MWB; I, ECP46MWB; Se, ECP28MWB)[24] and a (5s5p1d)/[3s3p1d]-DZ+P basis set.[25] For Nb a quasi-relativistic pseudopotential (ECP28MWB)[26] and a (8s7p6d)/[6s5p3d] basis set was used.[26] The computations were carried out at the DFT level using the hybrid method B3LYP which includes a mixture of Hartree−Fock exchange with hybrid DFT exchange-correlation. Becke's 3 parameter functional where

(19) Visser, J. W. *J. Appl. Crystallogr.* **1969**, *2*, 89.
(20) Altomare, A.; Burla, M. C.; Cascarano, G.; Giacovazzo, C.; Guagliardi, A.; Moltineri, A. G. G.; Polidori, G. J. *J. Appl. Crystallogr.* **1995**, *28*, 842.
(21) Altomare, A.; Cascarano, G.; Giacovazzo, C.; Guagliardi, A.; Burla, M. C.; Polidori, G.; Camalli, M. J. *J. Appl. Crystallogr.* **1994**, *27*, 435.
(22) Larson, A. C.; von Dreele, R. B. *General Structure Analysis System*; Los Alamos National Laboratory, Report LAUR 86-748: Los Alamos, NM, 1990.
(23) Frisch, M. J.; Trucks, G. W.; Schlegel, H. B.; Scuseria, G. E.; Robb, M. A.; Cheeseman, J. R.; Zakrzewski, V. G.; Montgomery, Jr., J. A.; Stratmann, R. E.; Burant, J. C.; Dapprich, S.; Millam, J. M.; Daniels, A. D.; Kudin, K. N.; Strain, M. C.; Farkas, O.; Tomasi, J.; Barone, V.; Cossi, M.; Cammi, R.; Mennucci, B.; Pomelli, C.; Adamo, C.; Clifford, S.; Ochterski, J.; Petersson, G. A.; Ayala, P. Y.; Cui, Q.; Morokuma, K.; Malick, D. K.; Rabuck, A. D.; Raghavachari, K.; Foresman, J. B.; Cioslowski, J.; Ortiz, J. V.; Stefanov, B. B.; Liu, G.; Liashenko, A.; Piskorz, P.; Komaromi, I.; Gomperts, R.; Martin, R. L.; Fox, D. J.; Keith, T.; Al-Laham, M. A.; Peng, C. Y.; Nanayakkara, A.; Gonzalez, C.; Challacombe, M.; Gill, P. M. W.; Johnson, B.; Chen, W.; Wong, M. W.; Andres, J. L.; Gonzalez, C.; Head-Gordon, M.; Replogle, E. S.; Pople, J. A. *Gaussian 98*, Revision A.6; Gaussian, Inc.: Pittsburgh, PA, 1998.
(24) Schwertfeger, P.; Dolg, M.; Schwarz, W. H. E.; Bowmaker, G. A.; Boyd, P. D. W. *J. Chem. Phys.* **1989**, *91*, 1762.
(25) Kaupp, M.; Schleyer, P. v. R.; Stoll, H.; Preuss, H. *J. Am. Chem. Soc.* **1991**, *113*, 1602.
(26) Andrae, D.; Häussermann, U.; Dolg, M.; Stoll, H.; Preuss, H. *Theor. Chim. Acta* **1990**, *77*, 123.

the nonlocal correlation is provided by the LYP expression (Lee, Yang, Parr correlation functional) was used which is implemented in Gaussian 98. For a concise definition of the B3LYP functional see ref 27.

Acknowledgment. We gratefully acknowledge the support of the Fonds der Chemischen Industrie, the Bundesministerium für Bildung und Forschung (Project 03-SC5LMU-5), the Deutsche Forschungsgemeinschaft (Gottfried-Wilhelm-Leibniz-Programm), and the University of Munich. We like to thank both referees for helpful and valuable comments.

(27) (a) Bauschlicher, C. W.; Partridge, H. *Chem. Phys. Lett.* **1994**, *231*, 277. (b) Becke, A. D. *J. Chem. Phys.* **1993**, *98*, 5648. (c) Becke, A. D. *Phys. Rev. A* **1988**, *38*, 3098. (d) Lee, C.; Yang, W.; Parr, R. G. *Phys. Rev. B* **1988**, *37*, 785. (e) Vosko, S. H.; Wilk, L.; Nusair, M. *Can. J. Phys.* **1980**, *58*, 1200.

Supporting Information Available: Tables giving computed and experimentally observed vibrational frequencies and their approximate assignments of $(P_4E_3)\cdot(BX_3)$ (E = S, Se; X = Br, I) and $(P_4Se_3)\cdot(NbCl_5)$ and X-ray crystallographic files, in CIF format, for the structure determinations of $(P_4S_3)\cdot(BBr_3)$ and $(P_4S_3)\cdot(BI_3)$. This material is available free of charge via the Internet at http://pubs.acs.org.

IC001384X